

F. ANGELINI

Nuclear Department
Physical Technologies and Security Division
Diagnostics and Metrology Laboratory
Frascati Research Centre, Rome - Italy

A COTS-based low-cost bistatic lidar for qualitative and semi-quantitative aerosol measurements

RT/2025/12/ENEA

ENEA

ITALIAN NATIONAL AGENCY FOR NEW TECHNOLOGIES,
ENERGY AND SUSTAINABLE ECONOMIC DEVELOPMENT

F. ANGELINI

Nuclear Department
Physical Technologies and Security Division
Diagnostics and Metrology Laboratory
Frascati Research Centre, Rome - Italy

A COTS-based low-cost bistatic lidar for qualitative and semi-quantitative aerosol measurements

RT/2025/12/ENEA



ITALIAN NATIONAL AGENCY FOR NEW TECHNOLOGIES,
ENERGY AND SUSTAINABLE ECONOMIC DEVELOPMENT

I rapporti tecnici sono scaricabili in formato pdf dal sito web ENEA alla pagina www.enea.it

I contenuti tecnico-scientifici dei rapporti tecnici dell'ENEA rispecchiano l'opinione degli autori e non necessariamente quella dell'Agenzia

The technical and scientific contents of these reports express the opinion of the authors but not necessarily the opinion of ENEA.

A COTS-based low-cost bistatic lidar for qualitative and semi-quantitative aerosol measurements

F. Angelini

Abstract

A low-cost, laser-based, instrument for liquid droplet detection and quantification has been set up and tested to evaluate the filtering efficiencies of some face masks. A full-frame Single Lens Reflex, equipped with a 100 mm F/2.8 macro, was installed in a forward scattering geometry to capture the small angle red light from a solid state laser diode (emitting at 650 nm) scattered from droplets emitted by an electric paint sprayer and crossing a face mask. The red channel of the pictures has been processed from the Nikon raw format (14-bit, lossless compressed) to ensure response linearity, and obtain the integrated scattering cross section of the cloud. The instrument, set up at home during the lockdown, was tested to estimate the filtering capability of facial masks, measuring the normalized amount of particles passing through different kinds of filtering masks. The results showed that the system is able to detect low quantities of droplets and also to provide imaging of the aerosol plume sections.

Keywords: lidar, aerosol, Covid-19, PPE.

Sommario

Uno strumento laser a basso costo per la rilevazione e la quantificazione delle goccioline liquide è stato messo a punto e collaudato con componenti commerciali e di basso costo. Il sistema è stato testato per valutare l'efficienza di filtraggio di alcune maschere facciali durante la pandemia da covid-19. Un reflex a lente singola full-frame, dotato di una macro F/2.8 da 100 mm, è stata installata in una geometria a scattering in avanti per catturare la luce rossa ad angolo ridotto proveniente da un diodo laser allo stato solido (che emette a 650 nm) disperso da goccioline emesse da uno spruzzatore di vernice elettrico e attraversando una maschera. Il canale rosso delle immagini è stato elaborato dal formato raw Nikon (14 bit, compresso senza perdita) per garantire la linearità della risposta e ottenere la sezione trasversale di dispersione integrata del cloud. Lo strumento, installato a casa durante il lockdown, è stato testato per stimare la capacità di filtrazione delle maschere facciali, misurando la quantità normalizzata di particelle che passano attraverso diversi tipi di maschere di filtraggio. I risultati hanno dimostrato che il sistema è in grado di rilevare piccole quantità di goccioline e anche di fornire immagini delle sezioni del pennacchio degli aerosol.

Sommario

1	INTRODUCTION	5
2	MATERIALS AND METHODS.....	6
2.1	Digital Single Lens Reflex	7
2.2	Laser level.....	8
2.3	Paint gun.....	9
2.4	Triggering system	10
2.5	Application to real scenarios	10
3	OPERATION AND RESULTS.....	10
4.1	3.1 Tested materials	11
4	POSSIBLE IMPROVEMENTS.....	12
4.1	Hardware	12
4.2	Software	13

1 INTRODUCTION

During the COVID-19 pandemic, the use of facial masks, available on the market in a variety of shapes and materials became diffused to slow down the diffusion of the viruses. However, in some periods and places the availability of such PPE was not ensured and improvised masks were built and worn. To estimate the efficiency of improvised masks a low cost lidar was designed, realized and tested on a set of facial masks to understand the performances of both a very simple bistatic home-made lidar and the different facial masks.

Studies in literature indicate that virus SARS-COV2, causing COVID-19, is mainly transmitted by respiratory droplets emitted when speaking, coughing, sneezing or simply exhaling [1], [2]; infection through contaminated surfaces is rather infrequent [3]. There are also many clues suggesting that virus diffuse indoor may be an active player of contamination [4], [5]. The efficiency of this kind of transmission is difficult to evaluate since depend on the droplet dimensions, their chemical composition which determine the speed of evaporation and, last but not least, the endurance of virus outside the organism. However, also the atmospheric aerosols might act as carriers to transport viruses and bacteria, though in this case the effectiveness of transmission strongly depends on the ability of microorganisms to resist in open air, at different temperature, humidity and solar radiation conditions [6]. In any case, restraint of droplets emitted by people is of course one of the best, and easiest, ways to limit contagion in crowded areas [7].

The easiest and most diffuse way to reduce the emitted droplets is the employ of facial masks, available on the market in a variety of shapes and materials. In fact, both the quantity of ejected material and the droplet size distribution are important for infection diffusion. The droplet size induces nonlinear effects in the virus survival probabilities: smaller droplets, that contain less virus load, evaporate quicker than larger droplets, further reducing the possibility of virus survival [8]. For this reason, face masks may help in reducing the risk of infection even if do not stop completely the flux ejected, for example by sneezing.

Some are specifically designed for a medical use [surgical masks], and filter out droplets emitted by normal breath, but do not assure high levels of filtering when sneezing [9]. In fact, the sealing of masks is not tested since the filtering efficiency is tested on a sample of material inserted at the entrance of a cascade impactor. In this way, no information on the overall efficiency of the device once worn is provided. Neither the filtering power of inhaled air is expected, exposing the wearer to breathing in contaminated aerosols.

On the other hand, filtering half masks to protect against particles (FFP1, FFP2 and FFP3 masks) are designed to filter out a large part of solid and liquid aerosols [10], but the devices to test this kind of PPE are very complex, expensive and then not suitable for fast and on-field operation. Moreover, these devices are thought to filter inhaled air, while exhaled air pressure is not considered as a main requirement.

In order to establish whether a face mask is efficient in holding back the droplets, here a simple laser-based instrument is presented and tested. and the ability to test leaks in filtering materials may be useful in developing countries or in situations where the availability of certified personal protection equipment (PPE) is not guaranteed.

A home-made bistatic lidar, constituted by a laser level, a digital single lens reflex (DSLR) camera and a paint gun (EPG) was built during Italian lockdown. Some components could be easily replaced with more performing ones, and a list of improvements will be discussed, as well as the possible methods for comparing the results with other measurements.

2 MATERIALS AND METHODS

The lidar system is here presented and discussed in terms of the single components. A CCD has been employed to frame the forward scattering of a laser line from a red laser level emitting at 650 nm impacting the droplets emitted by a paint gun. If a facial mask is inserted within the EPG and the laser line, the system is able to quantify the leaks of the masks in terms of optical cross section. A plastic bowl has been put around the nozzle to simulate a face where the masks can be worn for the trial. Thanks to the adopted Scheimpflug configuration [11], [12], the imaging of the laser line allows the integration of the signal over the whole droplet cloud and the consequent quantification of the signal scattered by integration over a region of interest (ROI) of the image recorded. A Mie scattering model can be employed to convert the cross section into mass, if the size distribution of the droplets can be assumed or measured: this possibility will be discussed as an improvement of the system. The scattering geometry is drawn in Figure 1.

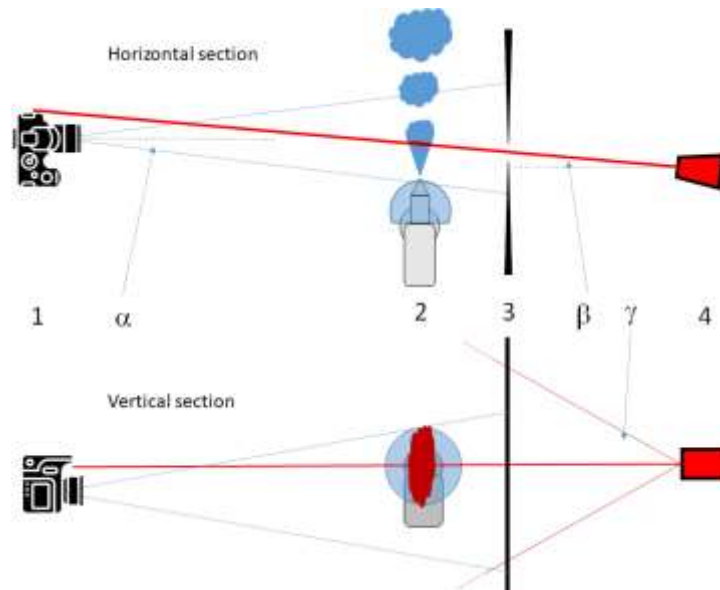


Figure 1. Cross sections of the layout. 1: Camera; 2: Paint gun with plastic bowl; 3. Screen; 4: laser level; α : camera field of view (20° vertical, 14° horizontal); β : laser tilt angle (5°); γ : laser divergence (vertical: 60°)

The camera, the nozzle and the laser are set on the same horizontal plane. The laser is tilted 5° with respect to the lens optical axis (β in Figure 1) to maintain a geometry that brings large cross section, without framing the laser source. In fact, two screens are placed near the laser path to exclude the direct exposure of the laser aperture and provide a homogeneous dark background for analysis. The laser line is oriented in a vertical plane that intercepts the spray from the paint gun: forward scattering between 4° and 6° is collected by the lens and forms an image onto the

CCD. Only Red channel is analyzed since the laser emission falls in the 635-670 nm, where Green and Blue pixel sensitivity is very low, while Red reaches its peak [13]. The laser is operated in continuous, while timing of paint gun and camera is managed by Arduino. Before discussing the results, a description of each component is given hereafter.

2.1 Digital Single Lens Reflex

A full-frame, 12 Mpx DSLR (Nikon D700) equipped with a macro lens (Tokina ATX 100 mm F/2.8) has been employed as sensor. The lens was manually focused at the distance of the spray gun.

CCDs are linear devices, where a charge is accumulated proportionally to the photons received by each pixel. Unfortunately, photographic data treatment does not preserve linearity of the output, since a variety of calibration curves are applied to the raw signal in order to obtain images more similar to classical chemical photography, and then darks, low lights, and highlights are processed to balance the histogram and make the image readable in each detail.

On the other hand, routines developed for astrophotography help in retrieving linear signals from raw picture. Nikon allows the picture processing at 14 bit and storage in lossless compressed ".NEF" raw format. Starting from these settings, a 48-bit tiff file can be obtained, and its augmented linearity and dynamic range result to be key points in the use of the camera as a lidar sensor. The DCRaw open source code [14] is conceived to provide linear output from raw camera images, and is used in many fields such as astrophotography, security, biology [15] [16] [17].

In this study in the Rawdrop Windows® executable program was used, embedding the DCRaw algorithm; each file was manually acquired, processed and analyzed. A direct implementation of the camera controls, the conversion algorithm and the analysis procedure will be implemented in a single control suite software, improving the easiness of use of the whole instrument. The linearity and dynamic range of the sensor was tested by averaging RGB levels of incremental exposures of the central part of a grey card, illuminated by 4000 K led lamps in a $2 \times 45^\circ : 0^\circ$ geometry. This configuration has been adopted to keep the processed image as homogeneous as possible, and results are shown in Figure 2. The advantage of using 14-bit storage settings coupled to the DCRaw processing algorithm is evident. All measurements have been carried out with the lowest ISO level (100 ISO) in order to keep the electronic noise as small as possible.

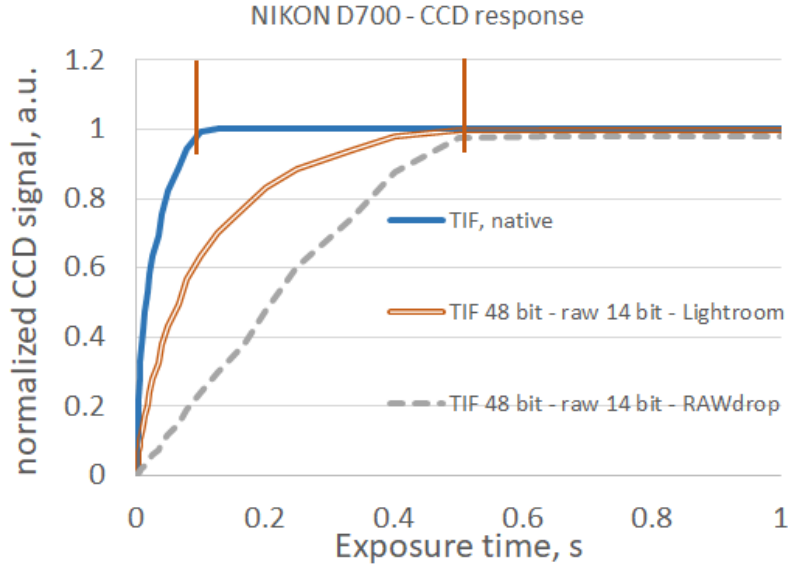


Figure 2. Dynamic range and linearity of sensor of TIF files: native, processed by Adobe Lightroom® and RawDrop software. The red lines represent the dynamic ranges achievable by the two methods. The superiority of post-production RAW-to-TIF conversion is evident, and the better linearity of DCRaw is also clearly visible.

2.2 Laser level

The laser beam was obtained by a commercial laser level (class 2M) emitting a laser line with a central brighter spot. Characteristics of the laser beam are summarized in Table 1. The use of a level instead of a simple laser pointer provides the interesting feature of illuminating all the section of the droplet cloud, allowing the measurement of the droplet integrated cross section. This eliminates the uncertainty coupled to sampling only a line of the cloud, although the chance of neglecting side spray is still possible.

Product	Wavelength	Power	Divergence
Black and Decker LZR310	635-670 nm	<3.5mW	60°

Table 1. Declared laser characteristics

In order to test the laser homogeneity, a picture of the laser line projected over a white homogeneous screen has been captured and is shown in Figure 3, together with the analysis of its intensity profile. F/8 lens aperture was selected to reduce vignetting of the picture, and the signal level of red channel was calculated as a vertical average of 64 pixels framing the laser line, once subtracted the background noise selected in the surrounding dark region.

As a first approximation, the profile was considered uniform; however, a future refinement should take into account the shape of the intensity profile to normalize each pixel of the picture to the relative laser line intensity in that point, quantity that depends on the angular distance from the central beam. For easiness and robustness of use, a polynomial fit is performed on the profile, excluding the central peak, to obtain an easy normalization curve.

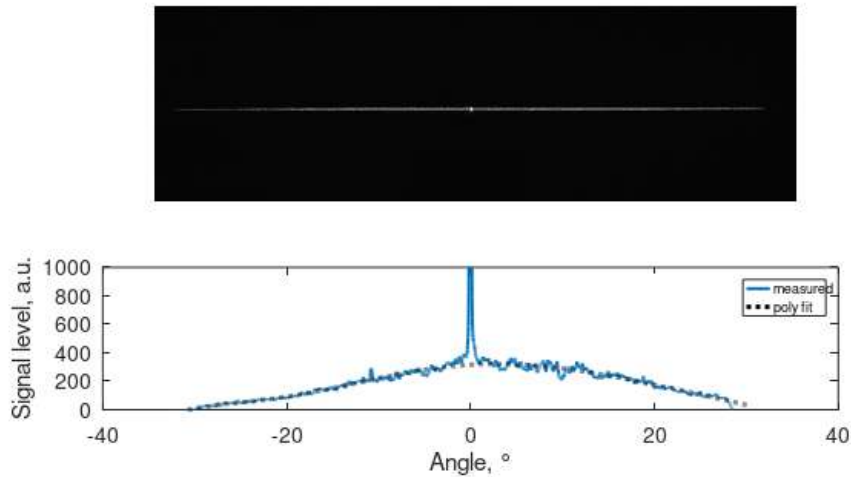


Figure 3. R channel (up) of the laser beam image with related intensity profile (down). The central beam reaches 6900 units. A polynomial fit (8th degree) is shown in dotted line.

An alternative is to employ a more uniform laser line, using a spatial filter and/or a beam shaper. However, sensitivity studies should point out whether this strategy, involving more expensive components, would be convenient or not.

2.3 Paint gun

A commercial electric paint gun (Meterk, 400W) has been employed to simulate the emitted droplet cloud. Unfortunately, no pressure control is possible, but flux speed has been estimated by a movie recorded at 100 fps against a dark background in forward scattering configuration. Results showed that the speed at the nozzle is about 3 m/s. This value makes our trial comparable with results in literature, both for coughing and sneezing [18] [19], in particular under the so-called pulsation regime. The first studies by Wells [20] report sneezing speeds as high as 100 m/s. On the other hand, Tang et al. [21] found 4-5 m/s to be the typical speed as maximum exit velocity, at least for their trial volunteers. In any case, our jet simulates physiological conditions, while strong sneezing acts would cause quite different pressure conditions inside the mask that should be well investigated before attributing leaks to the mask material rather than the sealing characteristics. Of course, the system proposed can be used for this purpose, once equipped by a suitable ejection system. The nozzle was oriented to obtain an elliptic section, vertically oriented to maximize the intersection area in the dimension not compressed by perspective in the Scheimpflug configuration. The tank was filled with distilled water, and the gun nozzle was inserted in a pierced plastic bowl, over which the masked were fixed, simulating a face. This is an important aspect, designed to create an excess pressure inside the mask and avoid the fluid to bypass the mask and freely exit from the sides.

2.4 Triggering system

The paint gun and the camera were triggered by Arduino-based circuit. Since the camera requires a short circuit on the front connector to expose, a couple of relays has been employed and separately driven by Arduino to start the paint gun and the camera. The delay between the spray and the exposure has been set to 940 ms since the gun requires about 0.7 s to start spraying after power connection. In this way, a fully developed cloud is captured by the snapshot before too much liquid is deposited on the mask. The whole system is manually triggered by pressing a button at each trial.

2.5 Application to real scenarios

One may wonder how representative the conditions in the experiment with respect of real conditions are. Real conditions cover a very wide range of situations: people may breathe normally, talk, yawn, cough or sneeze. The speed of ejected particles as well as their dimensions may be extremely different. A recent study [22] describe an instrument to simulate coughs of human ill patients, while others [23] [24] focused on the effects of facial shields on preventing diffusing and inhaling droplets caused by sneezing. The problem was faced either by numerical simulation or by experimental approach. In particular, [24] employs a system similar to the one proposed in this study, but using smoke particles to generate a cloud easier to visualize than liquid droplets. This variety of approaches witnesses, on the one hand, the importance of the topic and, on the other hand, the difficulties to scale the results to a real scenario. In any case, since we focused on the worst case of high-speed particles, the results could be considered as a lower bound of real performances. As already mentioned, though the paint gun used in the experiment cannot vary the pressure, the measured speed values are comparable with the literature. However, the possibility to validate the measurements is crucial to evaluate the real capability of the system. This aspect will be investigated with more detail in section 4.3.

3 OPERATION AND RESULTS

Once the system was set, two kinds of background measurements were performed to test the zero conditions for reference. Because of the possibility of uncontrolled fluctuations in the ambient illumination, a Dark Background (DB) is calculated for each frame, as the signal average in a region where no laser scattering is expected. Since intensity from different sources is additive, this value is subtracted from each image. Subtracting the DB also makes the integration insensitive to the size of the ROI.

The first reference was calculated with laser on and no spray. A small amount of signal was detected, due to scattering on dust particles. This value, averaged over 10 acquisitions was used as a Scattering Background (SB), subtracted of its DB and subtracted to each frame as shown in eq. (1).

The second kind of reference was obtained with laser on, spray on, and no mask interposed between the nozzle and the laser. This test provides the

value of cross section to be used as Normalization Factor (NF) for the tests, once subtracted of its own DB and SB values.

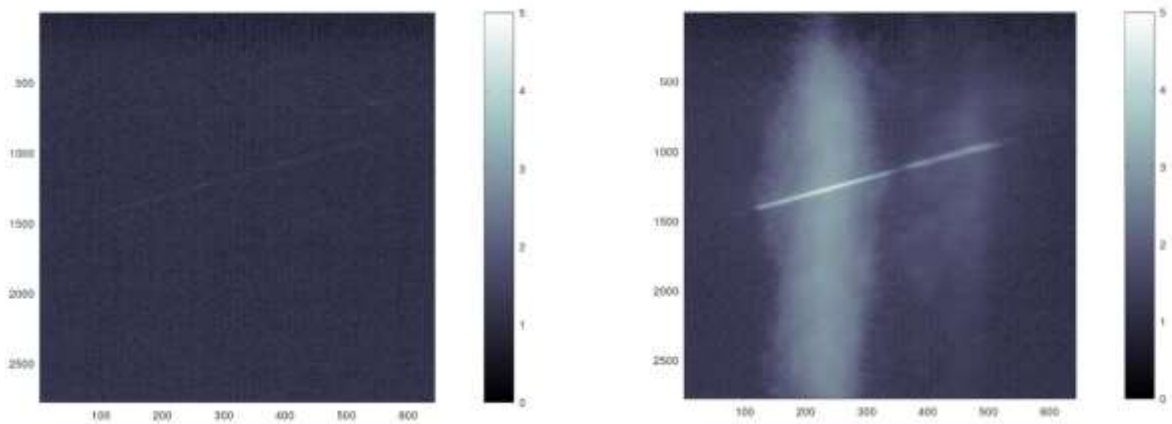


Figure 1. SB (left) and NF (right) signals obtained as averages of 10 frames each. The units are expressed as the \log_{10} (signal). the apparent slant path of the central brighter part of the laser line is given by the perspective as drawn in Fig. 1.

Both NF and SB signals, resulting as averages of 10 exposures, are shown in Figure 1. The exposure parameters were set so that the maximum pixel value in each frame used for NF never reached saturation ($2^{16}=65536$); the maximum value obtained was 61607. The camera was operated at 1/30 s, ISO 100, F/3 with 100 mm lens.

After the characterization of the zero conditions, the trials were repeated with several kinds of facial masks interposed between the nozzle and the laser. The signal S was integrated over the region shown in Figure 1, then dark subtracted and normalized by the NF. **Errore. L'origine riferimento non è stata trovata.** summarizes the values obtained for the references SB and NF.

Ref. type	Trials	Spray	Laser	S a. u.	DB a. u.	Rel. err. %
SB	10	No	Yes	21.8	14.3	2.9
NF	10	No	No	203.2	14.5	5.6

Table 2. Reference values NF and SB, with their DB values and relative errors, calculated from the standard deviations from single frames.

The resulting efficiency factor (EF) for the n-th sample is then calculated as:

$$EF_n (\%) = \frac{S_n - DB_n - SB}{NF} \cdot 100 \quad (1)$$

All the data analysis was performed with free GNU Octave language [25].

4.1 3.1 Tested materials

The masks were tested once fixed in front of the plastic bowl. Three measurements for each category have been carried out, changing sample at

each trial, since the water emitted by the EPG might alter the characteristics.

The samples tested together with the results of the analysis are described in Table 3. Six different mask types have been tested: half face dust mask (A), surgical mask (B), FFP3 mask with valve on side (C), single use dual layer (viscose+polyester, D), cotton sewed with cellfloc filter (E), single layer cotton jersey (F). Each type has been tested in three different samples, and the average result has been considered.

Tria ls	Spra y	Lase r	Mask	S a. u.	SB a. u.	EF %
3	Yes	Yes	A	21. 9	14. 3	0.01
3	Yes	Yes	B	21. 2	14. 4	-0.33
3	Yes	Yes	C	21. 7	14. 9	-0.36
3	Yes	Yes	D	21. 6	13. 8	0.22
3	Yes	Yes	E	21. 8	14. 5	-0.12
3	Yes	Yes	F	45. 0	14. 6	12.67

Table 3. Results of the measurements and reference conditions

As reported in Table 3, transmission can be considered null for all kinds but the single layer jersey mask, which shows about 13% of transmittance.

4 POSSIBLE IMPROVEMENTS

The lidar instrument was set up with the material available at home during the lock-down period. Some improvements can be brought both in hardware and in software components; however, the cost-benefit balance should be evaluated with respect to the precise goal of the experiment. Finally, the possibility to compare the results with other methods will be discussed.

4.1 Hardware

As stated, the paint gun did not allow any pressure control, nor measurement of differential pressure between the ambient inside and outside the mask. A more precise triggering system could be easily designed by using a paint gun working with compressed air, coupled to an electrovalve installed before the air nozzle. The electrovalve can be easily controlled by Arduino, and allows a more immediate and controllable spray.

Moreover, if a more sophisticated spraying system is adopted, the knowledge of the droplet size distribution could represent an important parameter to couple the results with a Mie model and retrieve the scattering-mass conversion factors. However, this is beyond the scopes of this work, since it is strongly dependent on the spraying device.

Improvements can be adopted also for the laser device. Many line lasers are commercially available nowadays, or a beam shaper could be adopted to form a line from a point laser. In case a very precise and homogeneous line is requested, a spatial filter can be set at the output of the laser. Also in this case, costs and benefits should be analyzed to better point out the best trade-off.

4.2 Software

As for the software, still a variety of improvements is possible, depending on the exact purpose of the instrument.

First, all the functions could be managed by a single computer, embedding the command of triggers, the acquisition of the camera frame and the analysis.

Inhomogeneity of the laser intensity could be taken into account by normalizing each pixel by the angular distance from the laser axis. This requires a careful alignment and measurement of the distances among the different components. This was beyond the scopes of this work, although represents a possible improvement for future uses. On the contrary, normalization by distance is not so important since the scattered cloud is very localized. If a longer path is employed, and a larger cloud is imaged, radiometric measurements should also take into account the attenuation of the laser beam (due to its divergence) and of the signal (due to the spherical dilution). If a larger zone is framed, also the difference in the scattering phase function should be considered, although this requires the knowledge of the droplet size distribution. In this case, the Mie theory can be used to determine the best angle range for scattering and the different normalization [26]. Mie theory was developed to compute the cross section and the phase function of dielectric spheres of arbitrary size, being useful in particular when spheres have size comparable with the wavelength of incident light. The use of laser radiation becomes particularly convenient because of its monochromaticity, so that Mie calculations become easier and more reliable. The aspects concerning the utility of Mie calculations will be discussed hereafter.

4.3 Calibration/validation of the system

Of course, an important point for the applicability of the technique lies in the possibility to compare the results with other measurements, for example as described in the cited UNI EN regulations, concerning the methods for determining the filtering classes of face masks. However, that kind of classification is related to the ability of dust filtration, and the measurements are based on impactors and other components that work exclusively with solid particles. Therefore, comparing results obtained on liquid droplets is actually a hard task since no reference methods have been established so far. A solution might come from techniques used in cloud sampling, used since the '40s, and refined since then [27] [28]. The basic idea consists in letting the droplets impact on a suitably coated surface [coated by metal oxides, soot ...] to reveal the diameter of the droplets, and then to analyze the traces through the microscope. Nowadays, automated measurements can be obtained by digital microscopes and pattern

recognition software, employed in many fields from medicine to agriculture [29] [30] [31].

This method allows determining the mass of leaks and the size distribution of fugitive droplets. Likely, the size distribution changes among different kinds of masks, so the sampling should be repeated and analyzed at each measurement: for this reason, automated recognition and analysis is crucial for reliable results.

In any case, the following guidelines can be sketched to allow the calibration of the system through the Mie theory. In fact, Mie theory can be employed to determine the function of scattering-to-mass conversion, as it is usually done in environmental lidar to retrieve the aerosol mass concentration from backscatter coefficient [32]. In this case, the refractive index is well known since it depends on the aerosol material [water], so the expected indetermination can be much lower especially if the size distribution of the spray has been determined. The Cal/Val of the instrument can be done by following this scheme:

1. Capture of droplets on a coated substrate;
2. Identification of droplets and size distribution computation;
3. Calculation of Mie cross section and phase function for the identified size distribution;
4. Estimation of scattering-to-mass coefficients.

However, since each of these steps requires developing dedicated calculations and software, an accurate Cal/Val procedure is beyond the scopes of the present work, and will be addressed in the future. However, laser instruments for measurement of the size distribution of droplets has been developed for industrial use, and some results have been published. A rough estimation of the size distribution of the aerosols produced by paintguns is reported in [33]; the authors found a diameter between 15 and 40 μm and resulted almost independent on the flow speed. This helps to conclude that the system is able to efficiently detect particles in this range and that almost all the face masks block most of them.

5 CONCLUSIONS

The build-up of a homemade low cost Sheimpflug lidar for the evaluation of the performances of facial masks is described and discussed. Limitations due to the pandemic period did not allow carrying out ancillary measurements necessary to validate the results or determine the calibration curve of the instrument.

However, all the tested facemasks, with the exception of the single layer jersey cotton mask, reported about 0% transmission at the test conditions. Even though some improvements can be implemented to enhance the performances, the proposed prototype has been able to detect leaks in at least one kind of filter, and can represent a useful tool for rapid or on-field testing of filters. A list of possible improvements is presented and discussed, as well as the roadmap for comparing the results with an independent and reliable method.

6 REFERENCES

- [1] Tang, S, et al. Aerosol transmission of SARS-CoV-2? Evidence, prevention and control. Environment international. 2020, Vol. 144.
- [2] Marquès, M and Domingo, J L. Contamination of inert surfaces by SARS-CoV-2: persistence, stability and infectivity. A review. Environmental Research. 2020.
- [3] Mondelli, M U, et al. Low risk of SARS-CoV-2 transmission by fomites in real-life conditions. The Lancet Infectious Diseases. 2020.
- [4] Morawska, L and Cao, J. Airborne transmission of SARS-CoV-2: The world should face the reality. Environment International. 2020, Vol. 105730.
- [5] Allen, J G and Marr, L C. Recognizing and controlling airborne transmission of SARS-CoV-2 in indoor environments. Indoor air. 2020, Vol. 30, 4.
- [6] Mohr, Alan Jeff. Fate and transport of microorganisms in air. Manual of Environmental Microbiology. Third Edition. s.l. : American Society of Microbiology, 2007, pp. 961-971.
- [7] National Academies of Sciences, Engineering, and Medicine. Rapid Expert Consultation on the Possibility of Bioaerosol Spread of SARS-CoV-2 for the COVID-19 Pandemic (April 1, 2020). Washington, DC: The National Academies Press. 2020.
- [8] Dombrovsky, Leonid A, et al. Modeling evaporation of water droplets as applied to survival of airborne viruses. Atmosphere. 2020, Vol. 11, 9, p. 965.
- [9] UNI EN 14683.
- [10] UNI EN 149.
- [11] Brydegaard, M, et al. The Scheimpflug lidar method. Lidar Remote Sensing for Environmental Monitoring. s.l. : International Society for Optics and Photonics, 2017, Vol. 10406, p. 104060I.
- [12] Kouakou, B. K., et al. Entomological Scheimpflug lidar for estimating unique insect classes in-situ field test from Ivory Coast. OSA Continuum. 2020, Vol. 3, 9, pp. 2362-2371.
- [13] De Miguel, S. A., et al. ISS nocturnal images as a scientific tool against light pollution: Flux calibration and colors. Highlights of Spanish Astrophysics VII. Berlin : Springer, 2013, pp. 916-919.
- [14] [Online] <https://www.dechifro.org/dcraw/>.
- [15] Burger, H. C., Schölkopf, B. and Harmeling , S. Removing noise from astronomical images using a pixel-specific noise model. IEEE International Conference on Computational Photography (ICCP). s.l. : IEEE, 2011, pp. 1-8.
- [16] Rich model for steganalysis of color images. Goljan, M., Fridrich, J. and Coganne, R. s.l. : IEEE, 2014. 2014 IEEE International Workshop on Information Forensics and Security (WIFS). pp. 185-190.

- [17] Wide field-of-view daytime fluorescence imaging of coral reefs. Treibitz, T., et al. s.l. : IEEE, 2013. 2013 OCEANS-San Diego. pp. 1-5.
- [18] Ahmed, M., et al. The far-field of coughs produced by healthy and influenza-infected human subjects. Methodology. 2017, Vol. 23.
- [19] Prasanna Simha, P. and Mohan Rao, P. S. Universal trends in human cough airflows at large distances. Physics of Fluids. 2020, Vol. 32, 8.
- [20] Wells, W. F. Airborne Contagion and Air Hygiene: an Ecological Study of Droplet Infection. Cambridge : Harvard University Press, 1955.
- [21] Tang, J. W., et al. Airflow dynamics of human jets: sneezing and breathing-potential sources of infectious aerosols. PLoS One. 2013, Vol. 8, 4, p. e59970.
- [22] Lindsley, W. G., et al. A cough aerosol simulator for the study of disease transmission by human cough-generated aerosols. Aerosol Science and Technology. 2013, Vol. 47, 8, pp. 937-944.
- [23] Akagi, F., et al. Effect of face shield design on the prevention of sneeze droplet inhalation. Physics of Fluids. 2021, Vol. 33, 3, p. 037131.
- [24] Arumuru, Venugopal, Samantaray, Sidhartha Sanka and Pasa, Jangyadatta. Experimental visualization of sneezing and efficacy of face masks and shields. Physics of Fluids. 2020, Vol. 32, 11, p. 115129.
- [25] [Online] <https://www.gnu.org/software/octave/index>.
- [26] Ragucci, R., Cavaliere, A. and Massoli, P. Drop sizing by laser light scattering exploiting intensity angular oscillation in the Mie regime,. Particle & particle systems characterization. 1990, Vol. 7, 1-4, pp. 221-225.
- [27] Mazur, J. The number and size distribution of water particles in natural clouds. Met. Res. Pap. 1943, Vol. 109.
- [28] Durbin, W. G. Droplet Sampling in Cumulus Clouds. Tellus. 1959, Vol. 11, 2, pp. 202-215.
- [29] Font, D., et al. Counting red grapes in vineyards by detecting specular spherical reflection peaks in RGB images obtained at night with artificial illumination. , 2014, 108: . Computers and electronics in agriculture. 2014, Vol. 108, pp. 105-111.
- [30] Rathore, S., et al. Capture largest included circles: An approach for counting red blood cells. International Multi Topic Conference. Berlin : pringer, 2012, pp. 373-384.
- [31] Alomari, Y. M., et al. Automatic detection and quantification of WBCs and RBCs using iterative structured circle detection algorithm. Computational and mathematical methods in medicine. 2014.
- [32] Barnaba, F. and Gobbi, G. P. Lidar estimation of tropospheric aerosol extinction, surface area and volume: Maritime and desert-dust cases. Journal of Geophysical Research: Atmospheres. 2001, Vol. 106, D3, pp. 3005-3018.

[33] Rohlmann, S., Wigger, G., Bornemann, C. et al. Droplet Size Distribution in Sprays of Waterborne Paint. *Int Surf Technol* 13, 16-19 (2020). <https://doi.org/10.1007/s35724-020-0124-0>

ENEA
Servizio Promozione e Comunicazione
www.enea.it

Stampa: Laboratorio Tecnografico ENEA - Centro Ricerche Frascati
luglio 2025